

University of Mississippi

eGrove

---

Honors Theses

Honors College (Sally McDonnell Barksdale  
Honors College)

---

2008

## Abnormal Group Velocities of Ultrasonic Pulses in Aqueous Suspensions of Polymer Microspheres

Robert Evans Heithaus

Follow this and additional works at: [https://egrove.olemiss.edu/hon\\_thesis](https://egrove.olemiss.edu/hon_thesis)

---

### Recommended Citation

Heithaus, Robert Evans, "Abnormal Group Velocities of Ultrasonic Pulses in Aqueous Suspensions of Polymer Microspheres" (2008). *Honors Theses*. 2346.

[https://egrove.olemiss.edu/hon\\_thesis/2346](https://egrove.olemiss.edu/hon_thesis/2346)

This Undergraduate Thesis is brought to you for free and open access by the Honors College (Sally McDonnell Barksdale Honors College) at eGrove. It has been accepted for inclusion in Honors Theses by an authorized administrator of eGrove. For more information, please contact [egrove@olemiss.edu](mailto:egrove@olemiss.edu).

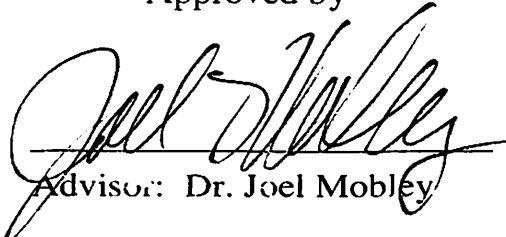
# Abnormal Group Velocities of Ultrasonic Pulses in Aqueous Suspensions of Polymer Microspheres

By  
**Robert Evans Heithaus**

A thesis submitted to the faculty of The University of Mississippi in partial fulfillment of the requirements of the Sally McDonnell Barksdale Honors College.

Oxford  
May 2008

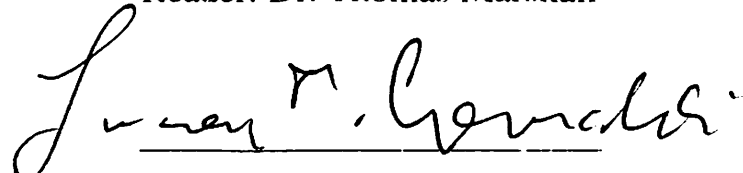
Approved by



Advisor: Dr. Joel Mobley



Reader: Dr. Thomas Marshall



Reader: Dr Lucien Cremaldi

## ACKNOWLEDGEMENTS

I would like to thank everyone who has helped me complete this project. Thank you to all of my friends who were supportive of me throughout this process, especially my dearest friend Stephen Altenbach. I would especially like to thank my thesis advisor, Dr. Joel Mobley. Without his patience and help I would have never been able to complete this project.

## ABSTRACT

ROBERT EVANS HEITHAUS: Abnormal Group Velocities of Ultrasonic Pulses in Aqueous Suspensions of Polymer Microspheres.  
(Under the direction of Dr. Joel Mobley)

In this project acoustic waves were employed to measure dispersion properties of two suspensions of polymer microspheres that were believed to support superluminal group velocities. Broadband ultrasonic pulses were first used to study a suspension of microspheres with a mean diameter of 160 microns. The validity of the data was verified using Kramers-Kronig relations, and the attenuation, phase, and group velocity spectra were published (Mobley, 2007a). During the second phase of the project a pulse consisting of broadband and narrowband components were propagated through the same 160 micron sample. The data are depicted in the Results section. Phase II studied several different bandwidths for each center frequency of the narrowband portion of the pulse. Finally, for Phase III the 160 micron suspension was replaced with a 100 micron suspension. A different range of center frequencies and bandwidths were employed for the narrowband portion of the pulse. As in Phase II the pulses contained both broadband and narrowband components. At each phase of the project attenuation, phase velocity, and group velocity were all examined and compared. Superluminal (i.e., faster than light) group velocities were calculated for certain frequency bands in each suspension. Although the group velocity was found to exceed the speed of light, relativity was not violated.

## TABLE OF CONTENTS

ABSTRACT.....	iii
LIST OF FIGURES .....	v
INTRODUCTION .....	1
MATERIALS AND METHODS.....	10
RESULTS .....	19
DISCUSSION .....	32
CONCLUSION.....	41
REFERENCES .....	42

## LIST OF FIGURES

Figure 1: Three sections of the sonic spectrum.

Figure 2: An illustration of the Gaussian windowed narrowband pulse and the signal envelope drawn around that pulse.

Figure 3: An illustration of the difference between a broadband and a narrowband pulse.

Figure 4: Photograph of one face of the custom sample chamber.

Figure 5: A schematic depicting the experimental set up for the through sample and the reference acquisition steps as well as the electronics used to acquire the data for Phase I of the project.

Figure 6: A photograph of the water tank with the transmit and receive immersion transducers. The sample chamber is in place between the two transducers.

Figure 7: A schematic depicting the experimental set up for both the through sample and the reference acquisition steps as well as the electronics used to acquire the data for Phase II and Phase III of the project.

Figure 8: An example of the signal used for Phase II and Phase III.

Figure 9: The attenuation spectra of the 160 $\mu$ m microsphere suspension used in Phase I of the project.

Figure 10: The phase velocity spectrum of the 160 $\mu$ m microsphere suspension used in Phase I of the project.

Figure 11: The group delay spectrum of the 160 $\mu$ m microsphere suspension used in Phase I of the project.

Figure 12: The group delay spectrum (left) and the group velocity magnitude (right).

Figure 13: The signal loss spectrum for Phase II of the project.

Figure 14: The phase time delay spectrum for Phase II of the project.

Figure 15: The group time delay spectrum for Phase II of the project.

Figure 16: The portion of the signal loss spectrum in which narrowband signals were employed.

Figure 17: The portion of the phase delay spectrum in which narrowband signals were employed.

Figure 18: The portion of the group delay spectrum in which narrowband signals were employed.

Figure 19: The attenuation spectrum for Phase III of the project.

Figure 20: The phase velocity spectrum for Phase III of the project.

Figure 21: The group delay spectrum for Phase III of the project.

Figure 22: A comparison of the group velocity and phase velocity of the broadband component of the signals employed in Phase III.

Figure 23: A comparison between the broadband and narrowband attenuation measurements for the Phase III data.

Figure 24: A comparison between the broadband and narrowband attenuation measurements for the Phase III data.

Figure 25: An expanded look at the group velocity data.

Figure 26: A comparison of the group delay spectrum of Phase I of the project with a Kramers-Kronig relation.

Figure 27: A ratio comparison of narrowband and broadband attenuation data for each frequency and bandwidth combination employed in Phase II of the project.

Figure 28: A fraction difference comparison of narrowband and broadband attenuation data for each frequency and bandwidth combination employed in Phase II of the project.

Figure 29: A ratio comparison of narrowband and broadband group velocity data for each frequency and bandwidth combination employed in Phase II of the project.

Figure 30: A fraction difference comparison of narrowband and broadband group velocity data for each frequency and bandwidth combination employed in Phase II of the project.

Figure 31: A comparison of the broadband and narrowband group velocity measurements of Phase III of the project.

Figure 32: A comparison of the broadband and narrowband group velocity measurements of Phase III of the project.

## INTRODUCTION

An acoustic wave can generally be defined as a mechanical wave which occurs as the result of a disturbance created through vibrations imparted to a medium. In the case of this experiment these disturbances are created by a device known as a transducer. The transducer creates sound through the use of a piezoelectric element which converts electrical signals into vibrations and vice versa. In the experiments described in this work the transducer is immersed in a water bath and generates pressure fluctuations at the water-transducer interface resulting in a sonic pulse propagating through the host medium (i.e. water) at a speed characteristic of that medium (Kinsler, 2000). For water, the speed of sound is governed by the temperature of the water, and this speed is roughly 1.5 mm/ $\mu$ s at 20 °C (approximately 1 mile per second). Acoustic waves, like electromagnetic waves (e.g., light, x-rays, microwaves), can be characterized by a frequency  $f$  and a wavelength  $\lambda$ . The frequency and wavelength are related through  $f = v/\lambda$  where  $v$  is the speed of sound.

Acoustic waves can be classified according to their frequency, resulting in what is known as the acoustic spectrum. The measured acoustic spectrum can be divided into several sections, three of which are shown in Figure 1. Acoustic waves with frequencies ranging from 20 Hz to 20,000 Hz fall within the sonic band familiar to us because it is the region of human hearing. Waves with frequencies falling below 20 Hz are in the infrasonic band. Infrasound is usually produced through large scale events such as explosions or earthquakes. Waves with frequencies at the upper end of the spectrum are



in the ultrasonic band. Ultrasound has proven to be extremely useful in various scientific and industrial applications. Ultrasound used in this project contains frequencies which range from 2 MHz to around 20 MHz or higher. The low MHz region of the ultrasonic spectrum is sometimes called the biomedical region since this includes the range used for diagnostic imaging and in some therapeutic applications. Unlike sonic and infrasonic waves, ultrasound is primarily studied in liquids and solids. The host medium in this project is water. Ultrasonic waves propagating in water with frequencies ranging from 2 to 20 MHz have wavelengths ranging from about 0.75 to 0.075 mm.

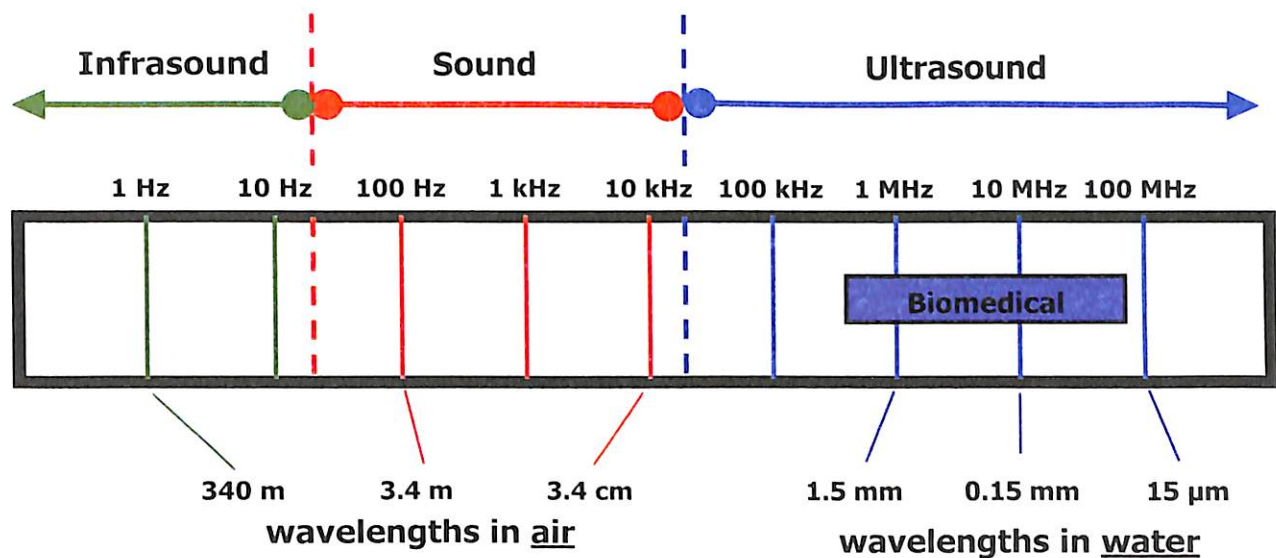


Figure 1: Three sections of the acoustic spectrum. Waves in the central section with frequencies ranging from 20 Hz to 20,000 Hz fall in the sonic band. Waves with frequencies falling below 20 Hz are in the infrasonic band, and those with frequencies above 20,000 Hz are in the ultrasonic band.

The focus of this project is the dispersive properties of ultrasonic waves transmitted through a suspension of scatterers. Dispersion refers to the variation in the properties of a wave, such as a wave speed, as a function of frequency. These suspensions can be strongly dispersive, greatly altering the wave's speed as a function of

frequency. Waves propagating in dispersive media can be described by up to five different velocities, each velocity describing a specific aspect of the wave (Brillouin, 1960). Of these, the most fundamental is the phase velocity. It represents the speed of the peaks or nadirs of a continuous sine wave as it travels through a medium. The phase velocity  $c_p$  is defined by the relation

$$k = \frac{\omega}{c_p} \quad (1)$$

where  $\omega$  is  $2\pi$  times the frequency and  $k=2\pi/\lambda$  is the real part of the complex wave number  $\kappa$  which is defined as

$$\kappa = k + i\alpha \quad (2a)$$

$$= 2\pi f / c_p + i\alpha \quad (2b).$$

The quantity  $\alpha$  is the attenuation coefficient (discussed below) is another intrinsic property of the bulk medium. As illustrated by equation 2b, the phase velocity and the attenuation coefficient are the fundamental components expressing the material properties in the complex wave number. In this project the phase velocity (as well as the group velocity) is reported in millimeters per microsecond (mm/ $\mu$ s) where the reference velocity—the speed of sound in water—is approximately 1.5 mm/ $\mu$ s.

Another aspect of signal propagation that plays an important role in this project is attenuation and the associated material parameter, the attenuation coefficient. Attenuation is a measurement of the energy redirected and/or absorbed from a forward directed propagating wave. The attenuation indicates how much of the original signal's energy is lost to, and redirected by, the medium through which the signal propagates.

The attenuation coefficient is especially important in this project because it provides for an alternate method of determining the phase and group velocities.

The second type of wave velocity studied in this project is the group velocity. The group velocity is unique because it can take on extreme and/or unusual values. It can be arbitrarily large and its magnitude can even go negative; alternatively it can also be extremely slow relative to the phase velocity. Generally speaking, an “abnormal” group velocity occurs when  $c_g$  is unusually large (e.g.,  $c_g \gg c_p$ ) or when the speed it represents becomes negative. In this project we report on the results of several experiments in which we attempted to directly measure and observe these extreme values for the group velocity.

In physics, the group velocity has been associated with the speeds of waves in various systems. In the case of quantum mechanics, where particles can also exhibit wavelike behavior, the group velocity has been associated with the speed of a group of particles. In the context of our work, the physical embodiment of the group velocity is with the speed of the envelope that describes the shape of a localized pulse of ultrasonic waves. But it is more complicated than this implies, as it only corresponds to the more general “envelope speed” under specific circumstances. The concept of a propagating wave group can be visualized by constructing a wave packet with multiple frequency components. An envelope can be drawn around this wave packet, and under the right conditions the speed of the envelope is described by the group velocity. The mathematical definition of the group velocity shown in equation 3,

$$\frac{1}{c_g} = \frac{dk}{d\omega} \tag{3}$$

A simple visualization of these wave envelopes is shown in Figure 2.

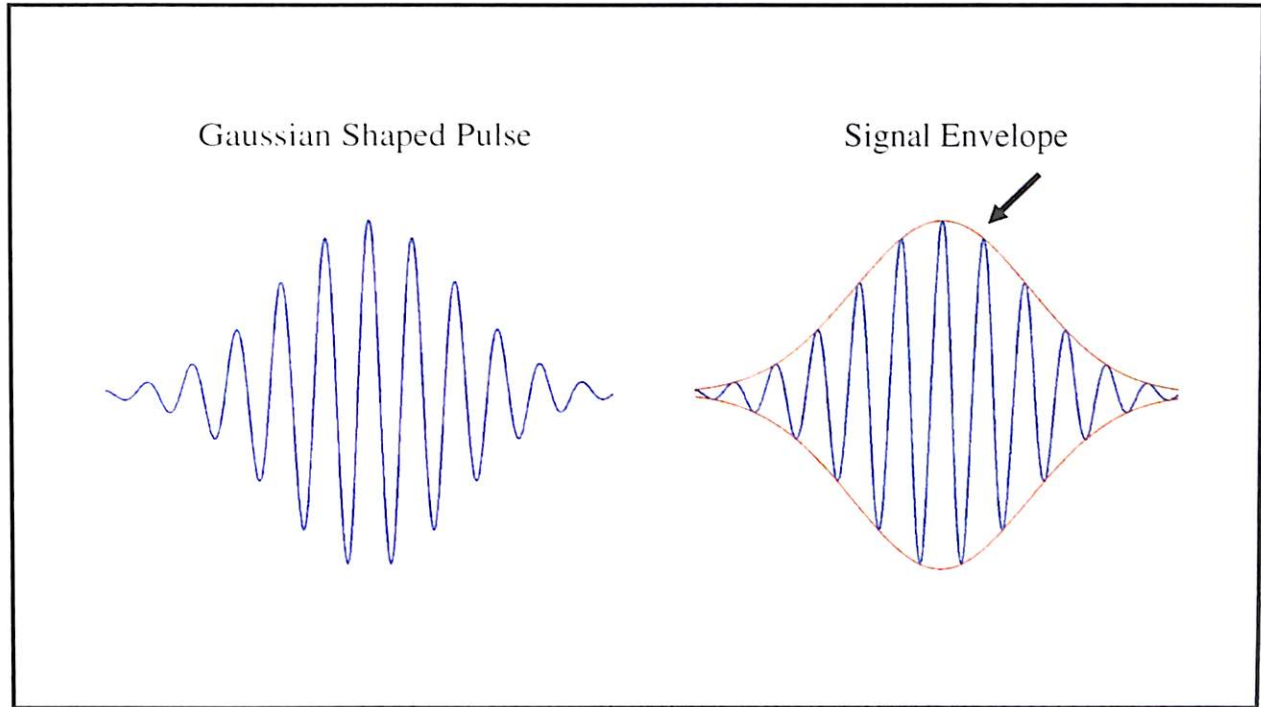


Figure 2: An illustration of the Gaussian windowed narrowband pulse and the signal envelope (in red) drawn around that pulse.

The group velocity can be derived from the phase velocity alone or from the attenuation coefficient using Kramers-Kronig techniques (Mobley, 1998). Although it can be visually observed by drawing envelopes over wave packets, the group velocity is defined mathematically through an expansion in a Taylor series of the real part of the complex wave number. The group velocity  $c_g$  is related to the phase velocity  $c_p$  by the following definition:

$$\frac{1}{c_g(\omega)} = \frac{1}{c_p(\omega)} \left( 1 - \frac{\omega}{c_p(\omega)} \frac{dc_p(\omega)}{d\omega} \right) \quad (4).$$

The properties described earlier (phase velocity, group velocity, and attenuation coefficient) can be measured in many different ways. In this project we used two different types of acoustic waves—broadband and narrowband—for the required

measurements. Time-localized (broadband) pulses are narrow in the time domain but broad in the frequency domain. Narrowband pulses are broad in the time domain but narrow in the frequency domain. Figure 3 illustrates the difference between a broadband and a narrowband pulse in both the time and the frequency domain (Note the difference in the horizontal scales of each pulse and its associated Fourier spectrum). Signals in this project are designated broadband because their bandwidths are large relative to the attenuation bands of the medium under study. The word “band” refers to a continuous range of frequencies in the acoustic spectrum. Thus the prefixes “narrow” and “broad” refer to the width of the acoustic spectrum occupied by the Fourier transform of the wave. The Fourier transform is a mathematical tool which effectively decomposes a signal into a collection of sine waves of different frequencies. Each sign wave component has its own amplitude and phase. The original signal can be reconstructed by adding together the sine waves with the amplitudes and phases determined by the Fourier transform. Fourier transformation is used in physics because it can simplify the analysis of the signals and the interpretation of the data for linear processes.

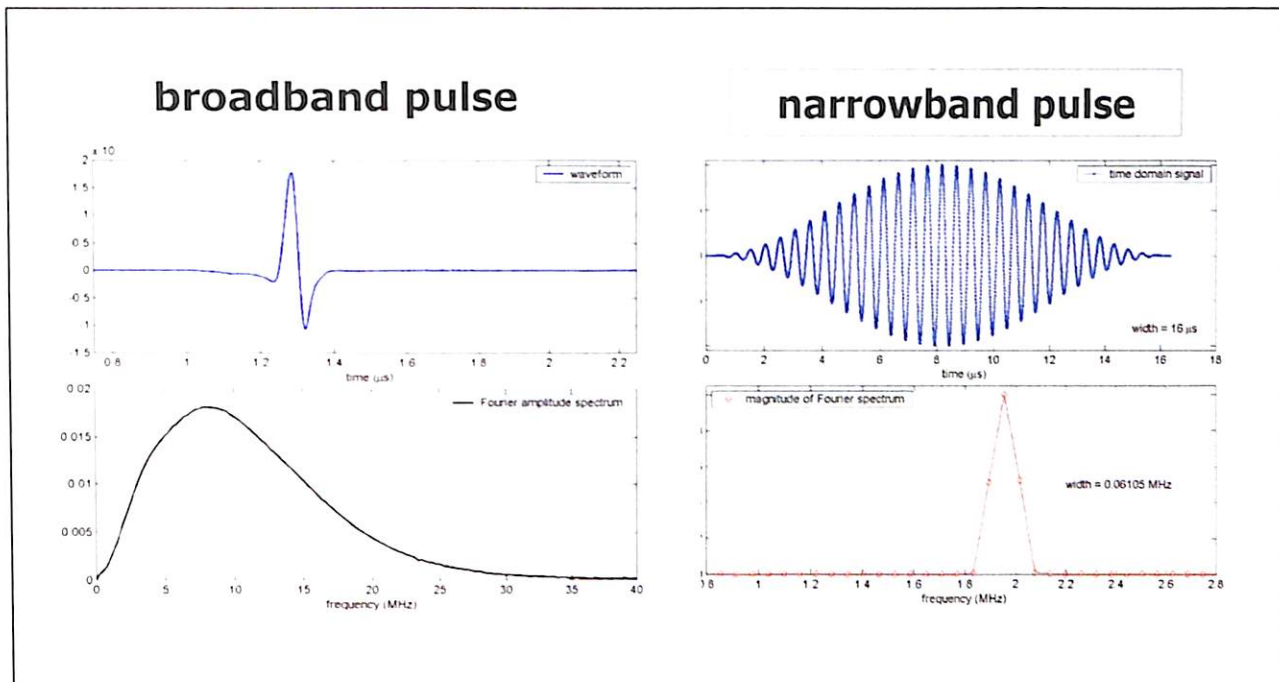


Figure 3: An illustration of the difference between a broadband and a narrowband pulse. The top two boxes display the signal in the time domain. The bottom two boxes show the Fourier spectrum of the respective signals. Broadband signals are narrow in time but broad in frequency. The opposite applies to narrowband signals. Note the difference in horizontal scales of each graph.

The experimental technique employed to acquire the necessary signals is similar for each type of signal (although there is a difference in signal processing steps for the narrowband and broadband methods). The measurements are performed using a simple substitution method where one signal is captured from propagation through a reference medium alone, and then the sample is substituted for some portion of the reference medium and a second signal is captured. The broadband and narrowband parts of the signals are then isolated and processed separately by time gating to obtain the group and envelope velocities respectively. In processing the broadband data, the gated broadband signals are Fourier transformed. The resulting Fourier transforms of the through-sample and reference signals are then compared in order to obtain the attenuation coefficient  $\alpha$

and the phase velocity  $c_p$ . The group velocity can then be calculated from the attenuation coefficient or the phase velocity.

For the narrowband data a signal envelope is determined from which the velocity of the peak of the envelope is derived. In some cases, we expect the narrowband envelope to move with the group velocity, but this will not be the case in general. To obtain the envelope velocity, signal envelopes are calculated using a Hilbert transform (Bracewell, 1986). The signal envelopes are then compared directly in order to obtain both signal loss (related to the attenuation coefficient) and the time delay between the signal peaks. This time delay can then be inserted into equation 5 to obtain the envelope velocity,

$$c_{peak} = \frac{c_{ref}}{1 - \frac{c_{ref}}{h} \Delta t} \quad (5)$$

where  $\Delta t$  is the time delay between the signal peaks and  $h$  is the sample thickness.

In order to obtain group velocities that were arbitrarily large or negative we had to select a sample that was sufficiently dispersive. Dispersion refers to the variation in the sample's phase velocity with respect to frequency (this is why we commonly write phase velocity as  $c_p(\omega)$ ). Apart from being sufficiently dispersive, the suspensions under study were selected because their ultrasonic properties closely match those predicted by an existing theoretical model (Mobley, 1999). The spheres were studied in solids volume fractions of approximately 3% in the suspensions. This volume fraction has been determined to be sufficient in order to create dispersive bands in the spectrum which exhibit the abnormal group velocities described earlier. The suspension is of special interest due to the fact that it exhibits multiple resonances in its scattering cross section

within the measurement bandwidth of our system. The resonance features are essential in obtaining abnormal group velocities which, in some cases, can become superluminal.

The word “superluminal” refers to speeds that are faster than the speed of light in vacuum. In order to adequately understand the physical manifestation of a superluminal group velocity it is necessary to understand that a velocity that is faster than light implies that it takes less time for a point of reference on a wave to appear at two different locations than it takes light to travel the same distance in vacuum. With this in mind it is sometimes easier to interpret data using the propagation times (i.e., group delays) rather than the group velocity. The group delay is simply the inverse of the group velocity, and it can be interpreted as “time of flight” per unit distance. This allows for negative speeds—or as we interpret through the data, negative delays. The idea of superluminal group velocities is not a new one. Since the early 1980’s a variety of systems have been producing superluminal group velocities, although in most cases it was done with electromagnetic waves (e.g., microwaves, light) (Mobley, 2007a). It’s important to note that the existence of superluminal velocities does not contradict Einstein’s theory of relativity which forbids the transmission of energy or information faster than the vacuum speed of light. Although these waves achieve superluminal velocities, it has been shown that inherent limitations of the phenomenon mean that information cannot be transferred at these speeds.

The remainder of this thesis will describe the details of the experiments, including construction and set up hardware, data acquisition and analysis. Additionally it will describe data for project Phases I, II, and III, and it will give a brief discussion of the wave properties revealed through the data.



## MATERIALS AND METHODS

### Project Phases

The project occurred in three phases. The Phase I employed the use of broadband techniques in order to identify a sample able to support superluminal group velocities. Phase II employed narrowband techniques to directly observe abnormal group velocities as well as broadband techniques to confirm narrowband measurements. Both Phase I and Phase II studied a sample of microspheres with a mean diameter of 160  $\mu\text{m}$ . Phase III of the project employed both broadband and narrowband techniques in order to study a second sample of microspheres with a mean diameter of 100  $\mu\text{m}$ . All three phases of the experiment used the substitution technique mentioned earlier to obtain the signal data.

### Microsphere Suspensions

The samples studied were composed of microspheres (Duke Scientific Corporation, Palo Alto, CA) made of polystyrene and/or polystyrene divinylbenzene suspended in an aqueous solution. The microspheres used NIST-traceable size standards and are typically used for the calibration of particle sizing systems because of their uniformity (the individual particle diameters only vary within a few percent of the mean). The aqueous solution in which the spheres were suspended contained a dispersant in order to prevent the microspheres from agglomerating. The microspheres were studied in suspensions with a 3% volume fraction—a volume fraction adequate for providing the dispersion necessary for the existence of the abnormal velocities (Mobley, 2007a).

## Apparatus

The sample was placed in a specially constructed chamber—pictured below in Figure 4—which created a region of containment for the microspheres. The sample chamber's windows were constructed using Saran Wrap approximately 25  $\mu\text{m}$  thick (Mobley, 1999). The Saran Wrap was used because it has been determined to be nearly acoustically transparent when using the through transmission technique. At first a standard lab wrap from Fisher Scientific was used for measurements; however, it was soon discovered that the lab wrap did not provide a sufficient seal to contain the microspheres for a long period of time in the sample chamber.

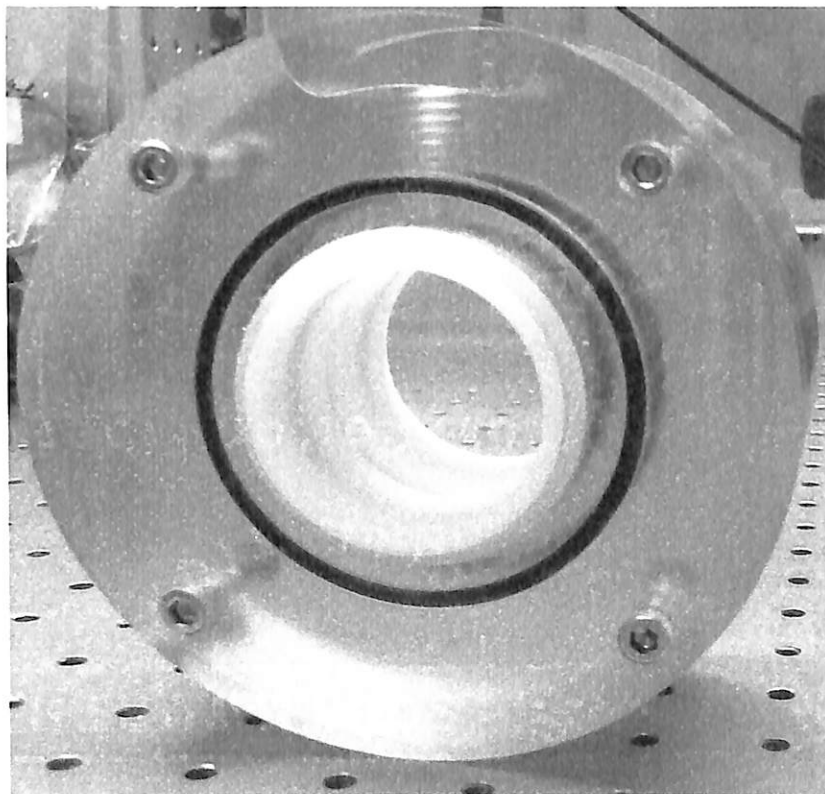


Figure 4: Photograph of one face of the custom sample chamber.

The sample chamber was modified from the specifications in \*Appendix X. Larger screws for each of the two side panels were used to obtain a better seal around the

o-rings. A 1/8 inch hole was bored in the sample chamber screw cap, and a small section of Tygon tubing (Cole-Parmer, Vernon Hills, IL) was inserted through the hole. The tubing was attached to a 200  $\mu$ L pipette through a standard plastic disposable pipette tip. The tubing was extended through the screw cap and immersed into the aqueous solution containing the microspheres. The sample was mixed continuously during waveform acquisition using a 200  $\mu$ L pipette. Earlier work had determined this mixing method to be adequate for measuring ultrasonic properties of polymer microsphere suspensions (Mobley, 1999 & Hall, 1996).

### **Data Acquisition**

In Phase I of the experiment broadband signals were generated using a Panametrics 5800 broadband pulser/receiver unit. These signals were transmitted from the pulser/receiver unit to one of two Panametrics PVDF focused transducers (2 in. focus, 0.25 in. active diameter). The transducers were mounted in specially constructed mounts connected to a rail-mounted system that utilized three micrometer stages and one rotational stage to achieve four degrees of freedom. This mounting technique was used because it allowed both gross and fine adjustment of transducer alignment. Because the transducers were focused, the alignment was critical for achieving maximal signal transmission during data acquisition.

The transducers, along with the sample chamber were submerged in a tank of degassed water. Because the velocity of sound in water varies with temperature, the tank water temperature was recorded at the beginning and end of each data acquisition session. Once the excitation signals were transduced into ultrasonic waves at the transmitting transducer, the wave packets propagated through the water, across the sample chamber,

and they were transduced back to electrical signals by the receiving transducer. The experimental setup is depicted in Figure 5.

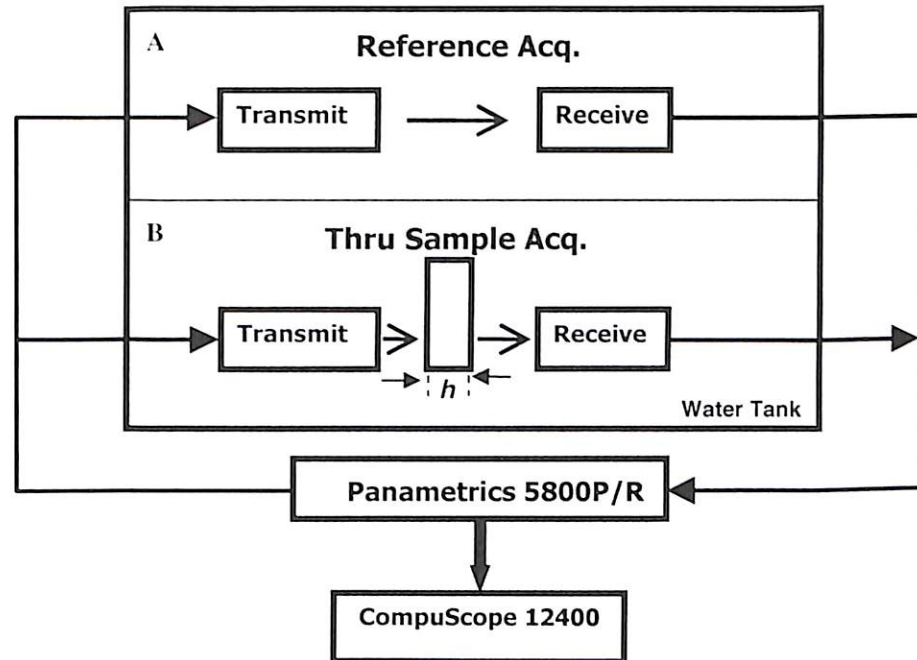


Figure 5: A schematic depicting the experimental set up for the through sample (B) and the reference (A) acquisition steps as well as the electronics used to acquire the data. This set up was used for Phase I of the project. Both measurements are performed under water. The only difference between the two acquisitions is the presence or absence of the sample.

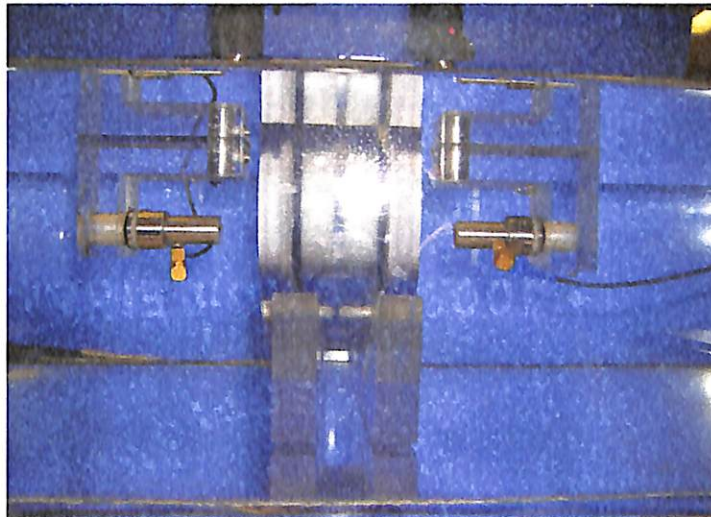


Figure 6: A photograph of the water tank (illustrated earlier in Fig. 5(B)) with the transmit and receive immersion transducers. The sample chamber is in place between the two transducers.

The waves collected by the receiving transducer were then amplified using the Panametrics 5800 broadband pulser/receiver unit. The data was digitized using a CompuScope 12400 (Gage Applied Technologies) PCI card running in 12-bit single channel mode at a sample rate of  $400 \times 10^6$  samples/s. During each acquisition many wave forms were averaged (ranging from several hundred to several thousand), and the resulting average was saved to a file. Data were then analyzed by reading the data from the files into Matlab using custom written software.

In order to determine all the necessary parameters four different waveforms had to be acquired. The reference waveform was taken with the sample chamber in place. During reference measurements the microspheres in the sample chamber were left undisturbed, allowing the microspheres to settle to the bottom of the chamber and out of the region of acoustical transmission (note: this region was small due to the focusing properties of the transducers). This reference measurement was later used in calculations in which the through sample waveform was compared with the reference waveform.

In addition to the reference waveform two pulse echo waveforms were taken to measure the sample thickness. These pulse-echo waveforms were acquired utilizing the pulse-echo function of the Panametrics 5800 broadband pulser/receiver unit. The pulse-echo technique is a method in which a pulse of ultrasound is both transmitted and received by the same transducer. An ultrasonic pulse is sent out of a transducer, and it is reflected off of the near wall of the sample. Once the pulse is reflected the echo wave travels back to the transducer. The propagation times of the reflections for each sample boundary and the through-transmission reference waveform, along with the velocity of sound in water (governed by the temperature), can be used to measure distances. The

pulse-echo signals taken from each transducer can determine the distance between each transducer and each wall of the sample chamber. Those two parameters can be subtracted from the total distance (determined by a through transmission reference wave) to determine the sample thickness  $h$ .

### **Narrowband Signals**

The experimental procedure for Phase II and Phase III was modified in order to include the acquisition of narrowband signals. Signals containing both narrowband and broadband components were generated using a CompuGen 4300 (Gage Applied Technologies) arbitrary waveform generator controlled by a personalized script running in Matlab (Math Works, Cambridge, MA, USA Version R2007a). These signals were used to excite the transmitting transducer, and the waves followed the same path as before. The modified experimental setup is depicted below in Figure 7.

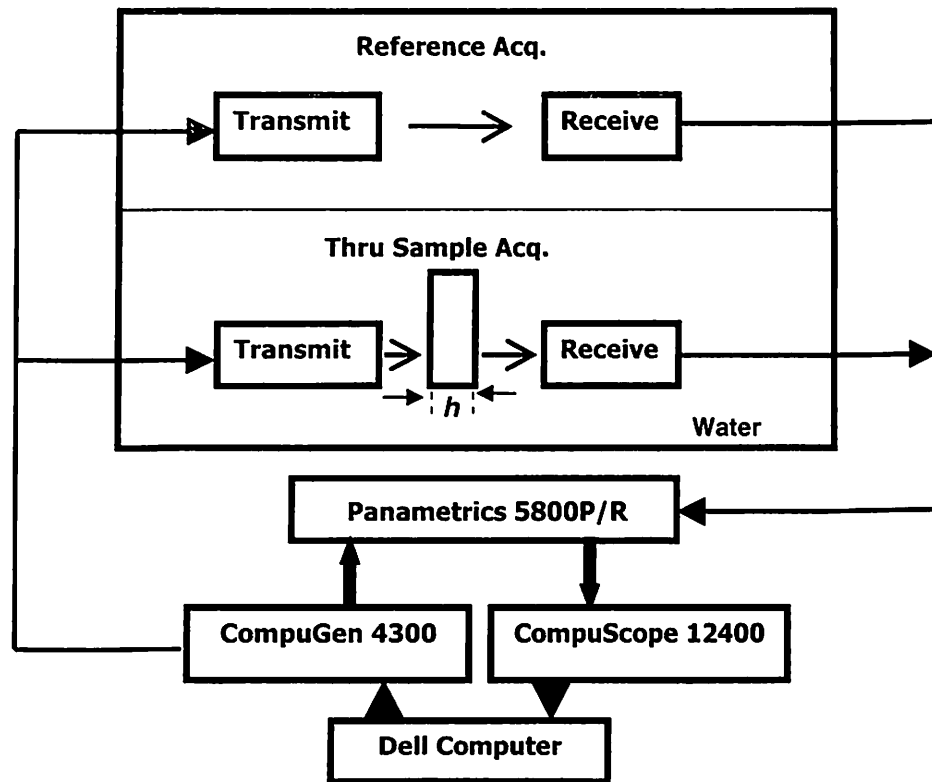


Figure 7: A schematic depicting the experimental set up for both the through sample and the reference acquisition steps as well as the electronics used to acquire the data. This set up was used for Phase II and Phase III.

During Phase II combinations of narrowband and broadband pulses were used in conjunction. The waves sent through the 160  $\mu\text{m}$  diameter microsphere suspensions contained both a leading narrowband component and a separate trailing broadband component (depicted in Figure 8). The center frequency of the narrowband signal was varied from 7.90 MHz to 8.30 MHz in increments of 0.10 MHz. Four different bandwidths were applied at each frequency. The bandwidths were 0.07, 0.10, 0.40 and 1.60 MHz leading to 20 different narrowband signals. These waveforms were collected, and the average of 2000 waveforms of each combination was saved for later analysis.

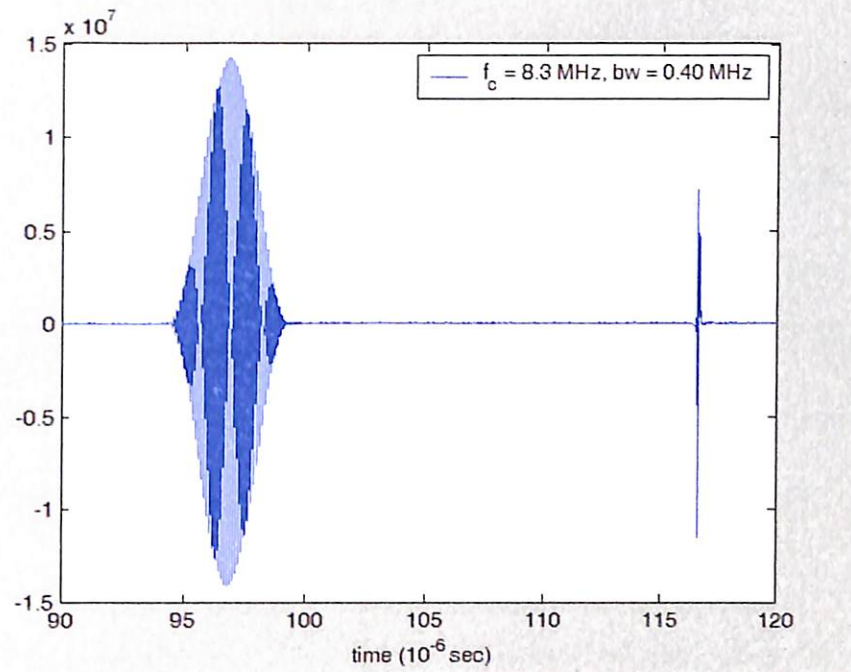


Figure 8: An example of the signal used for Phase II and Phase III. The signal has two components. The left portion of the signal contains the narrowband component, and the right portion of the signal contains the broadband portion of the signal.

Phase III involved not only a different sample but also a different set of signals. As mentioned earlier the sample was changed to a suspension containing 100  $\mu\text{m}$  diameter microspheres. A different set of frequencies and bandwidths were used. The center frequency of the narrowband signal was varied from 8.6 to 9.0 MHz and from 9.8 to 10.4 MHz in increments of 0.10 MHz. Two different bandwidths were applied at each center frequency leading to a total of 24 different narrowband signals. The two bandwidths were 0.10 and 0.40 MHz. The waveforms were acquired, and the average of 5000 waveforms of each combination was saved for later analysis.

### Data Analysis

In terms of the experimental variables determined in our project, the group velocity relation can be written as



$$c_g(\omega) = \left( \frac{1}{c_{g,ref}} - \frac{1}{h} \frac{d\Delta\Phi}{d\omega} \right)^{-1} \quad (6)$$

where  $\Delta\Phi = \Phi_{\text{thru}} - \Phi_{\text{ref}}$ , the  $\Phi$ 's are the phases of the Fourier transforms of the through sample and reference pulses,  $h$  is the thickness of the sample under study, and  $c_{g,ref}$  is the reference velocity of the waveform while propagating through the host medium alone (water) without the dispersive medium present (Mobley, 2007a). Attenuation is calculated by directly comparing the Fourier transforms of the reference wave and the wave that has passed through the dispersive medium. Equation 7 is the equation employed for the calculation of the attenuation coefficient, an inherent property of a bulk media, for each frequency that comprises the pulses.

$$\alpha(\omega) = \frac{\ln\left(\frac{A_{ref}(\omega)}{A_{thru}(\omega)}\right) - \ln T}{h} \quad (7)$$

The quantity  $\alpha$  is the attenuation coefficient which is a function of frequency  $\omega$ , and  $h$  is the sample thickness. The quantity  $A_{thru}$  is the amplitude spectrum of the Fourier transform of the signal from the through-sample acquisition and  $A_{ref}$  is the amplitude spectrum of the Fourier transform from the reference acquisition (Mobley, 2007a). Attenuation is sometimes reported in the dimensionless unit called the decibel (dB), and the attenuation coefficient is reported in dB per unit distance. This project reports the attenuation coefficient in nepers (Np) per unit distance. The neper is a dimensionless unit like the decibel; nepers utilize natural logarithms whereas decibels are defined in terms of base-10 logarithms.

## RESULTS

The results of Phase I are shown in Figures 9-12 (figures adapted from Mobley 2007). The attenuation coefficient and phase velocity spectra are shown in Figure 9 and Figure 10 respectively. The spectra show nine sharp peaks in the attenuation coefficient, the most prominent occurring near 4.5 MHz. The attenuation spectra vary from 0.03 Np/mm up to 1.07 Np/mm. The phase velocity exhibits behavior that is consistent with the attenuation spectra in the Kramers-Kronig sense. Near the region of 4.5 MHz the phase velocity drops to approximately 1.47 mm/ $\mu$ s. The velocity increases rapidly when moving higher in frequency to a region that corresponds to a low attenuation band seen in Figure 9. The phase velocity increases by 0.074 mm/ $\mu$ s through this region. The group delay spectrum is shown in Figure 11. The group delay exhibits three extreme delays occurring below 10 MHz. Near the region of 4.5 MHz there is an extreme drop in the group delay exhibiting a negative delay approaching  $-0.4 \text{ (mm}/\mu\text{s)}^{-1}$ . This region is shown in more detail in Figure 12. The second portion of Figure 12 is a logarithmic plot of the magnitude of the group delay versus the frequency. The magnitude of the group velocity exceeds the speed of light reaching  $4.34 \times 10^5 \text{ mm}/\mu\text{s}$  at one point. In the region surrounding 4.5 MHz the delay curve actually crosses zero indicating that the group velocity has the capability of exhibiting arbitrarily large values at the frequencies near the point where the delay curve crosses zero (Mobley, 2007a).

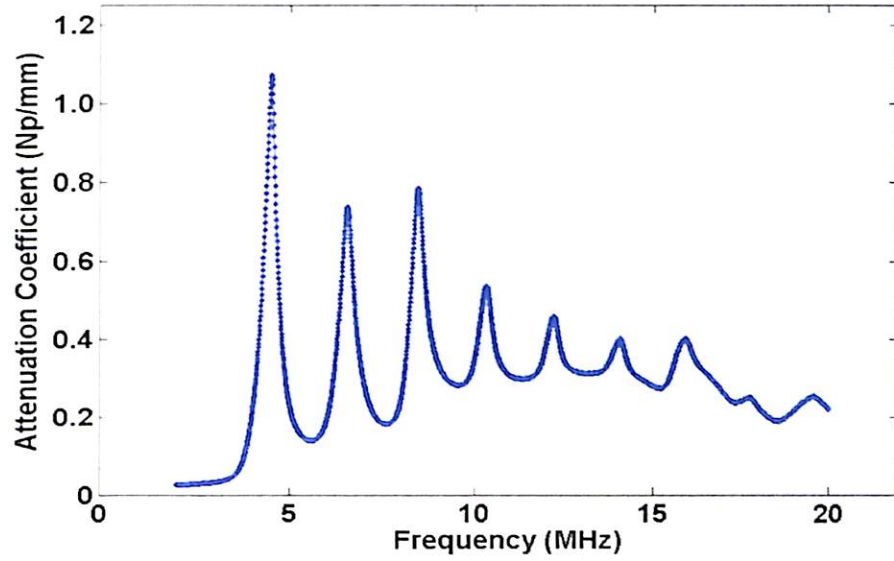


Figure 9: The attenuation spectrum of the 160  $\mu\text{m}$  microsphere suspension used in Phase I of the project. The spectrum shows nine peaks, the most prominent occurring near 4.5MHz (figure adapted from Mobley 2007).

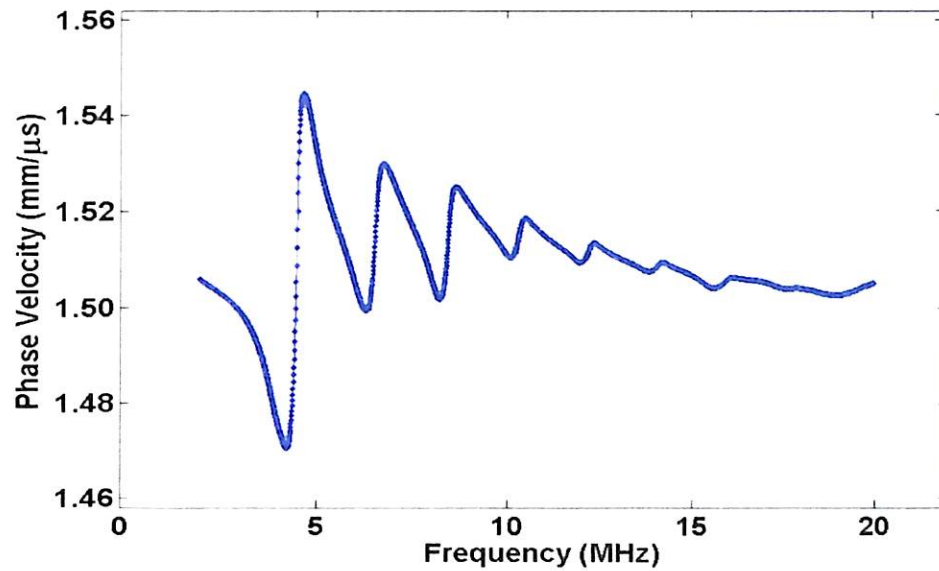


Figure 10: The phase velocity spectrum of the 160  $\mu\text{m}$  microsphere suspension used in Phase I of the project (figure adapted from Mobley 2007).

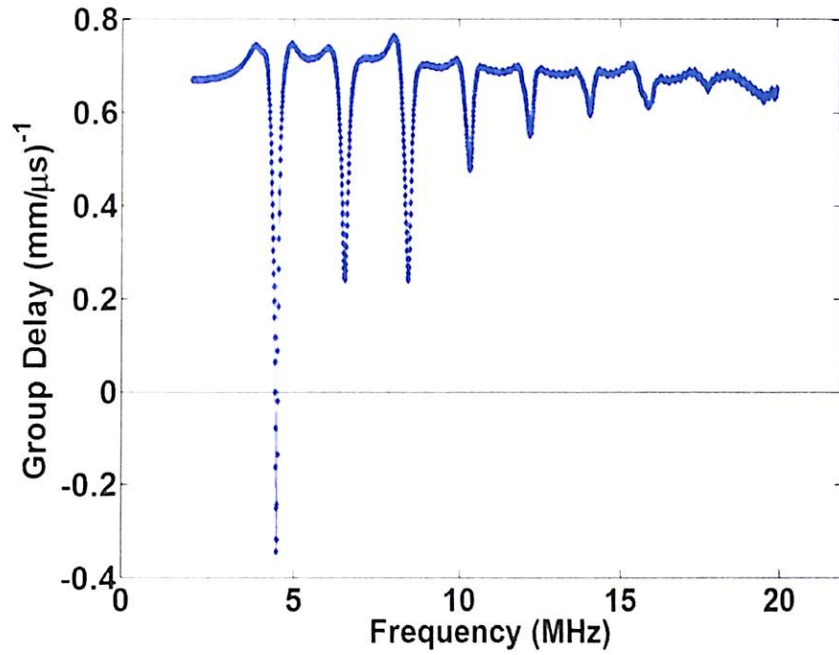


Figure 11: The group delay spectrum of the 160µm microsphere suspension used in Phase I of the project. The region exhibiting negative delay appears near 4.5 MHz (figure adapted from Mobley 2007).

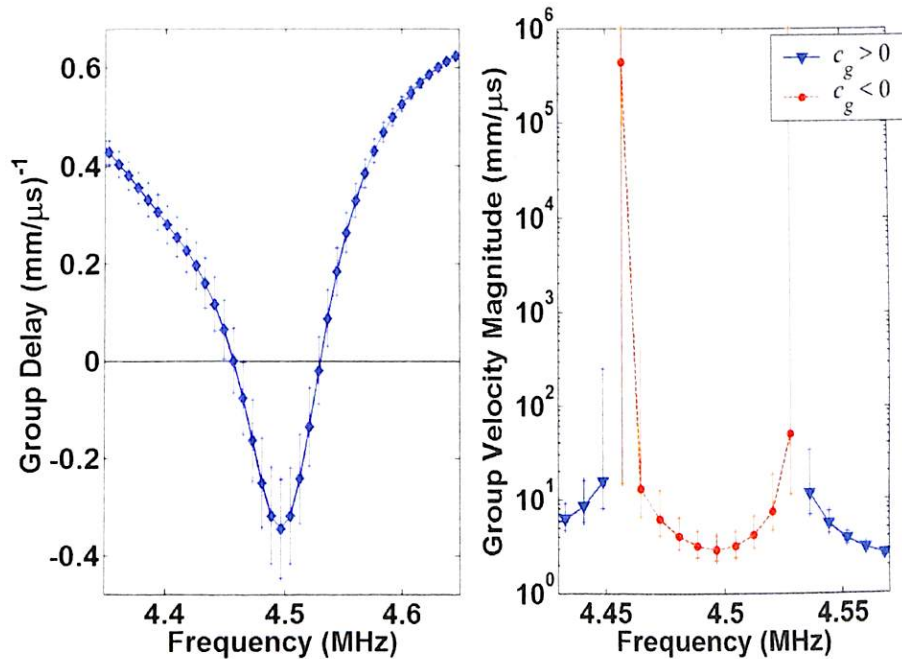


Figure 12: The group delay spectrum (left) and the group velocity magnitude (right). The group delay spectrum is focused on the region where the negative delay band occurs. The group velocity is plotted logarithmically revealing a maximum velocity of  $4.34 \times 10^5$  mm/µs at 4.46 MHz (figure adapted from Mobley 2007).

The data for Phase II is shown in Figures 13-15. Figure 13 shows the signal loss (i.e. attenuation) for the broadband portion of the pulse. The spectra show a prominent attenuation peak near 4.5 MHz along with several other peaks of lesser intensity. The phase time delay data is shown in Figure 14. From Kramers-Kronig relations, one expects that certain features in the attenuation coefficient spectra will be accompanied by certain structures in the phase velocity data. This is very similar to the relationship between magnitude and phase for a simple damped harmonic oscillator. Figures 16, 17 and 18 show the curve for the broadband data, and the diamonds located along each curve indicate the different center frequencies of the narrowband signals. The signal with a center frequency of 7.9 MHz falls in a region of low attenuation, and the signal with a center frequency of 8.3 MHz falls in a region of high attenuation. The attenuation of the frequencies in between varies, increasing as the frequency increases. For the group delay time the lower center frequencies fell in a region where the group delay was at a minimum.

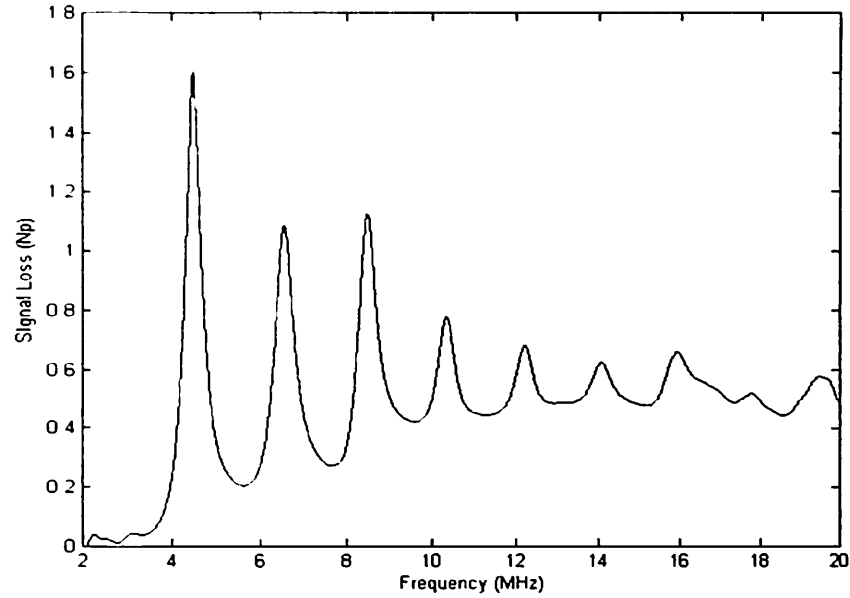


Figure 13: The signal loss spectrum for Phase II of the project. This signal loss spectrum exhibits a similar attenuation to that illustrated by Figure 8. This was anticipated due to the fact that the microsphere sizing was the same in both phases of the experiment.

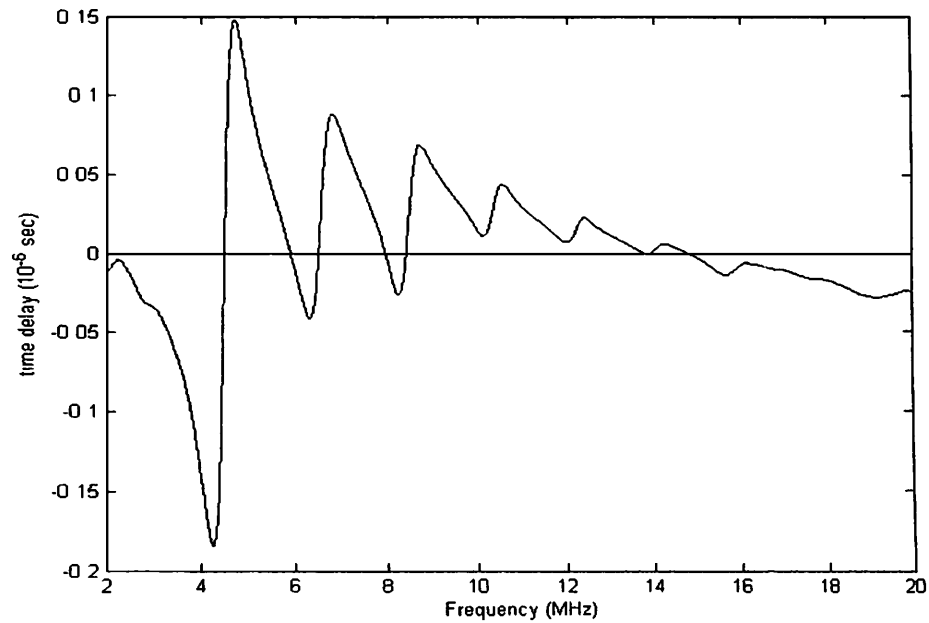


Figure 14: The phase time delay spectrum for Phase II of the project. The phase time delay spectrum exhibits behavior consistent with the signal loss spectrum.

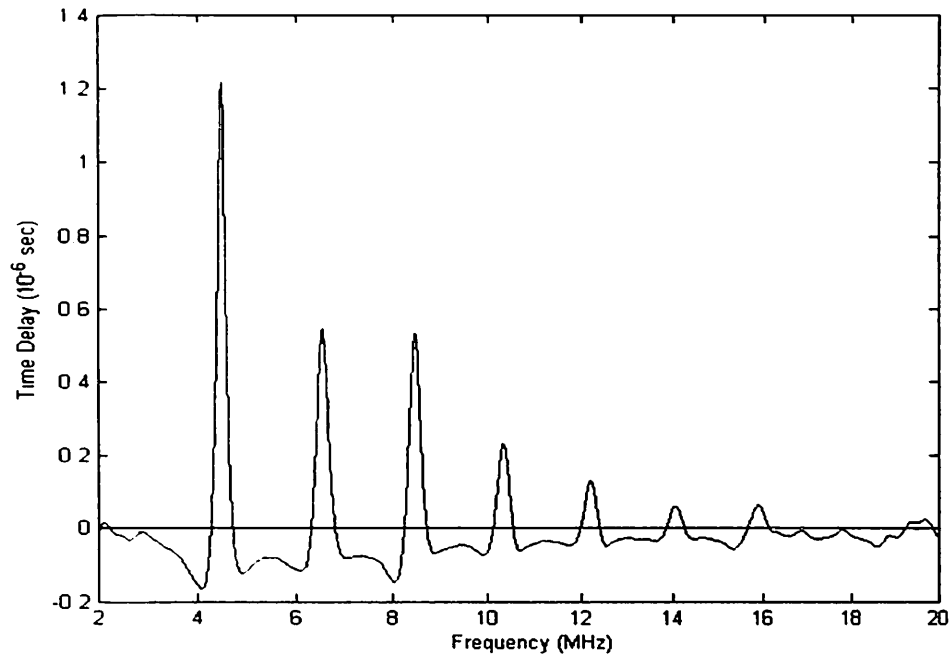


Figure 15: The group time delay spectrum for Phase II of the project. This figure is a comparison with the reference velocity of sound in water. The zero line does not indicate zero velocity; rather it is the delay of a reference pulse. These calculations do not indicate negative delays and subsequently superluminal velocities. Instead they depict group velocities that are slower than the reference velocity.

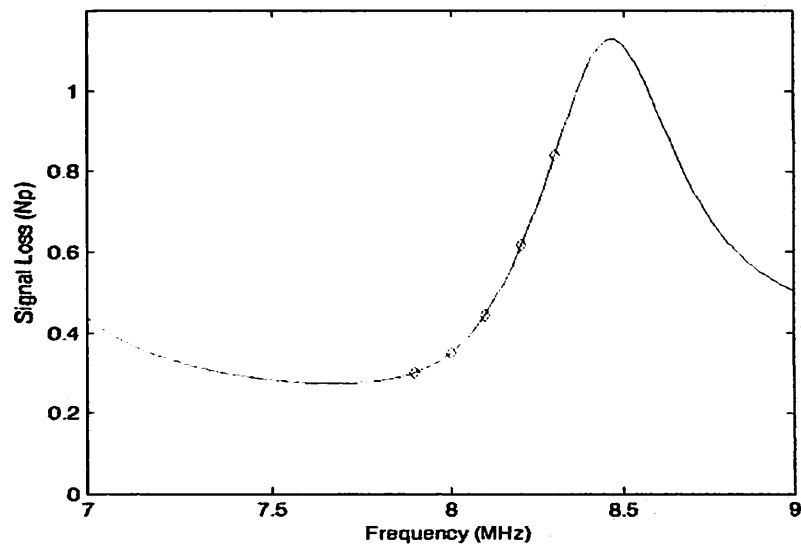


Figure 16: The portion of the signal loss spectrum in which narrowband signals were employed. The diamonds indicate the center frequencies of each narrowband signal where data was acquired. The diamonds appear at 7.9, 8.0, 8.1, 8.2, and 8.3 MHz.

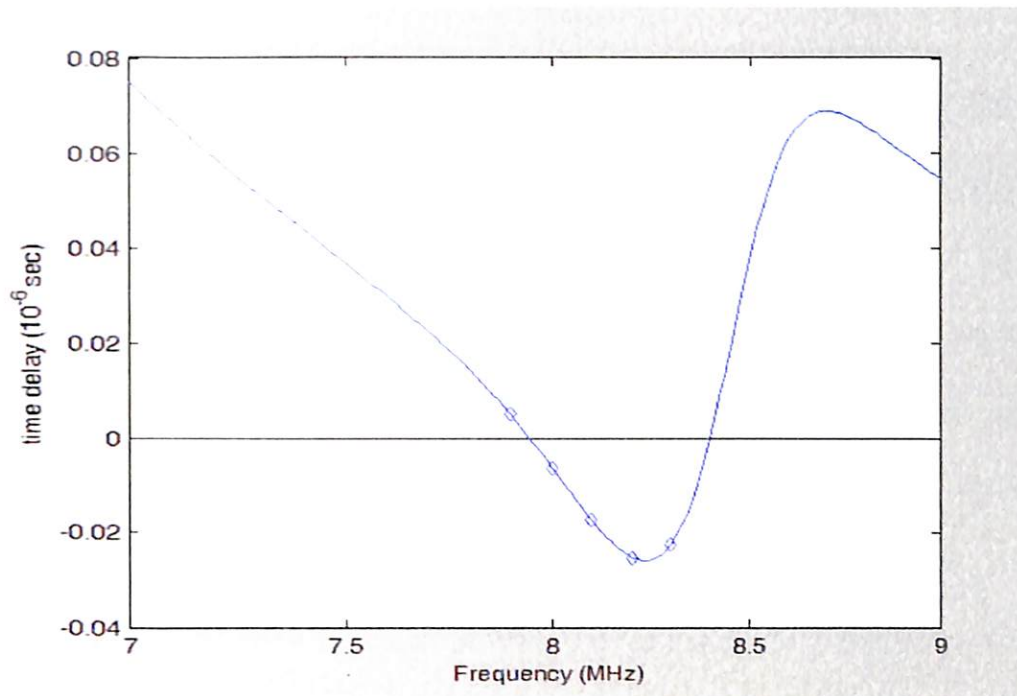


Figure 17: The portion of the phase delay spectrum in which narrowband signals were employed. The diamonds indicate the center frequencies of each narrowband signal where data was acquired. The diamonds appear at 7.9, 8.0, 8.1, 8.2, and 8.3 MHz.

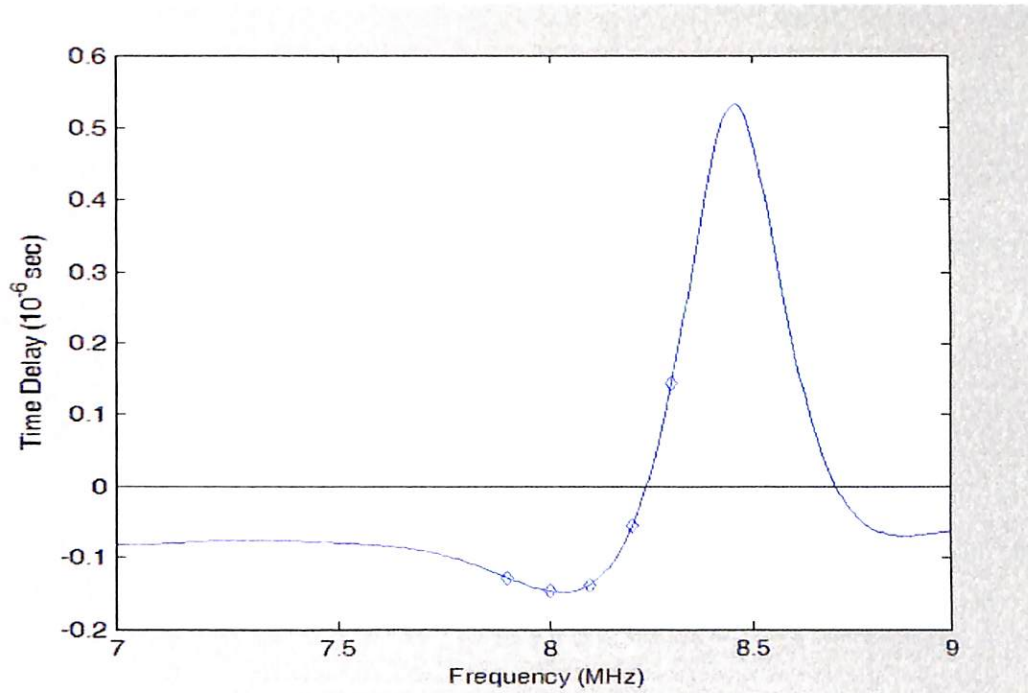


Figure 18: The portion of the group delay spectrum in which narrowband signals were employed. The diamonds indicate the center frequencies of each narrowband signal where data was acquired. The diamonds appear at 7.9, 8.0, 8.1, 8.2, and 8.3 MHz. The lower three frequencies occur in a region indicating slow group velocities, and therefore we should expect our narrowband data to reveal slower than normal group velocities.



Figures 19-22 show the data for Phase III of the experiment, the phase in which the 100 micron spheres were employed. The attenuation spectrum depicted in Figure 19 contains five peaks with the three most prominent peaks occurring near the regions of approximately 7, 10 and 13.5 MHz. The phase velocity spectrum is shown in Figure 20. Near the region of 7 MHz the phase velocity drops to nearly 1.44 mm/ $\mu$ s. As frequency increases the phase velocity rapidly increases corresponding to the first attenuation peak of the spectrum of Figure 19. This behavior is apparent several more times for the rest of the spectrum. The group delay spectrum is shown in Figure 21. The group delay exhibits three negative delays occurring below 14 MHz. In the region just above 10 MHz there is an extreme drop in the group delay exhibiting a delay greater than (more negative than) -1.0 (mm/ $\mu$ s)<sup>-1</sup>. Another extreme negative delay appears between 13 and 14 MHz. This delay is not as extreme as the one occurring just above 10 MHz, but the delay does approach -1.0 (mm/ $\mu$ s)<sup>-1</sup>. The broadband spectra for attenuation, phase velocity, and group delay show clear differences (shape, size and position of peaks) between the 160  $\mu$ m and 100  $\mu$ m diameter sphere suspensions.

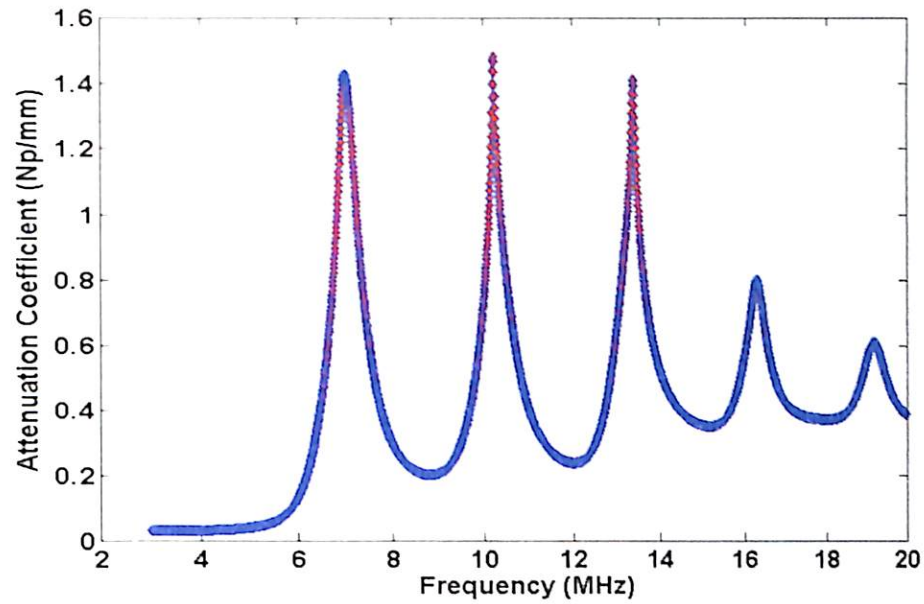


Figure 19: The attenuation spectrum for the 100 micron suspension taken in Phase III. The spectrum reveals five attenuation peaks with the most prominent three peaks occurring below 14 MHz.

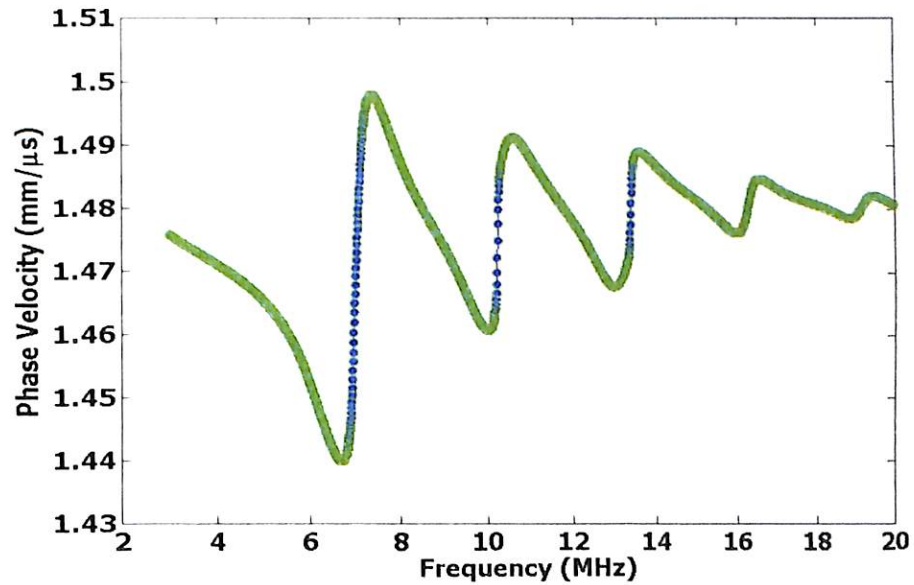


Figure 20: The phase velocity spectrum for the 100 micron suspension taken for Phase III of the project. Near the region of 7 MHz the phase velocity drops to nearly 1.44 mm/ $\mu$ s. As frequency increases the phase velocity rapidly increases corresponding to the first attenuation peak of the spectrum of Figure 19.

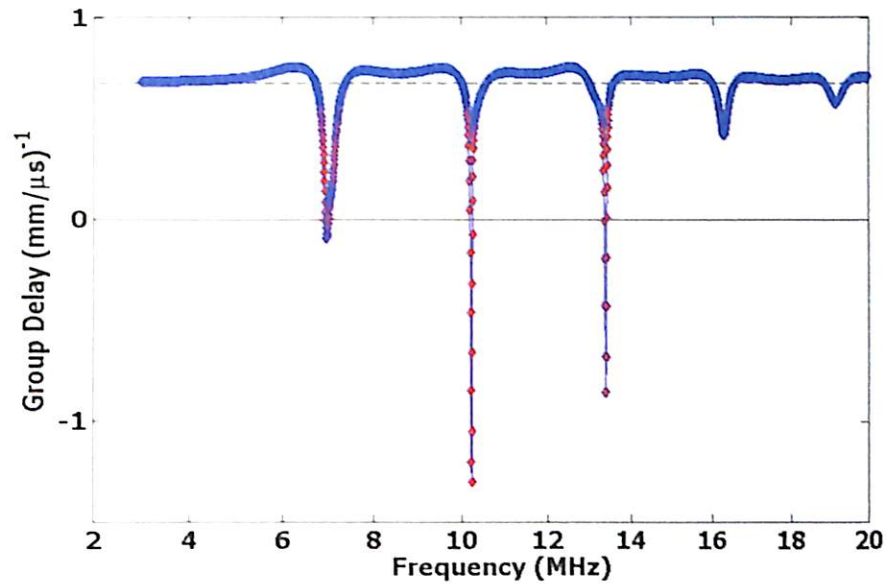


Figure 21: The group delay spectrum for Phase III of the project. The group delay exhibits three negative delays occurring near 7, 10 and 13 MHz with the most extreme delay greater than (more negative than)  $-1.0 \text{ (mm}/\mu\text{s)}^{-1}$ .

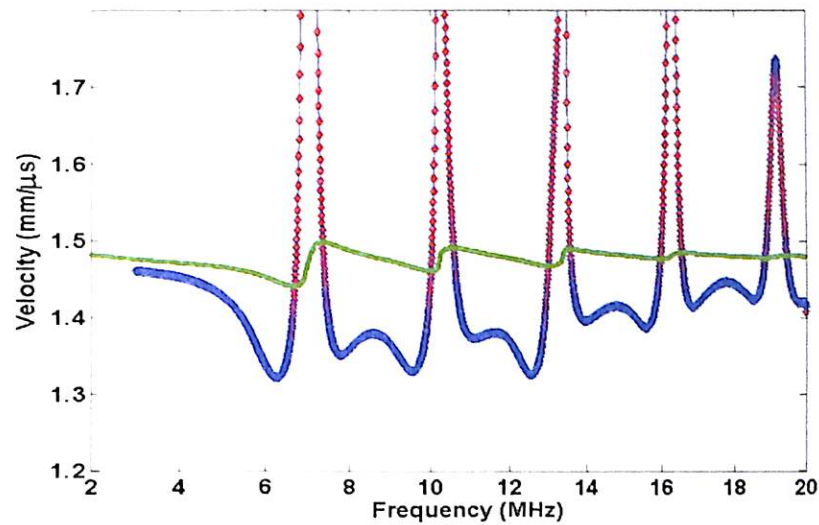


Figure 22: A comparison of the group velocity and phase velocity of the broadband component of the signals employed in Phase III of the project. The vast difference between the phase velocity (lighter shaded line) and the group velocity (darker line) are seen.

The data for the narrowband results are reported in Figures 23-25. Both bandwidths show agreement with the broadband data from 8.6 to 9.0 MHz in the attenuation spectrum. The data from 9.8 to 10.4 MHz shows a greater variation. Both bandwidths show a similar trend, but the signals with a bandwidth of 0.10 MHz show greater agreement with the broadband spectrum. The group and phase velocity comparisons are depicted in Figures 24 and 25. From 9.0 to 10.4 MHz the 0.1 MHz bandwidth data show a greater increase in the group velocity where as the 0.4 MHz bandwidth data show only a slight increase in the group velocity of this range of frequencies. When moving to the region of frequencies between 8.6 and 9.0 MHz the 0.4 MHz bandwidth data shows a higher level of agreement with the broadband data than does the 0.1 MHz bandwidth data.

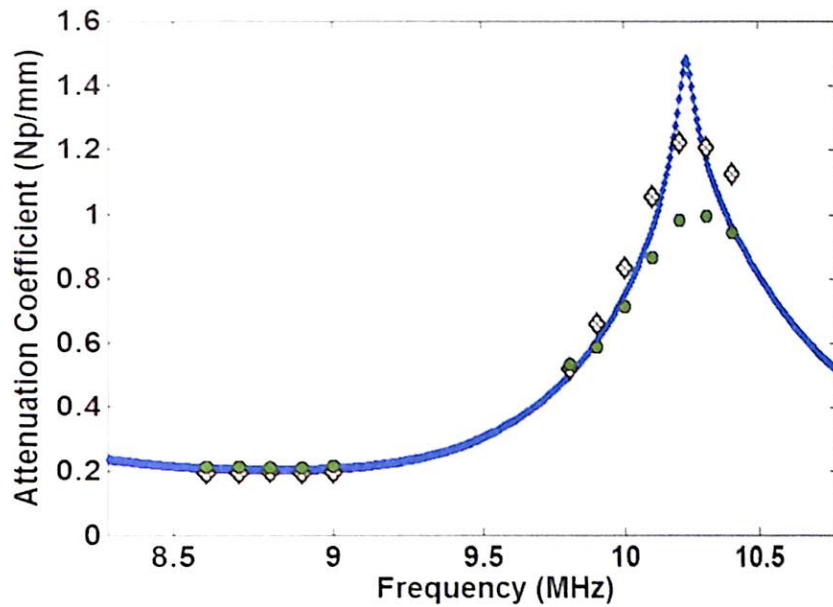


Figure 23: A comparison between the broadband and narrowband attenuation measurements for the Phase III data. The diamonds denote the center frequencies of the narrowband signals with a bandwidth of 0.10 MHz, and the dots denote the center frequencies of those signals with a bandwidth of 0.40 MHz. A high level of correspondence among the data is seen in the region between 8.6 and 9.0 MHz.

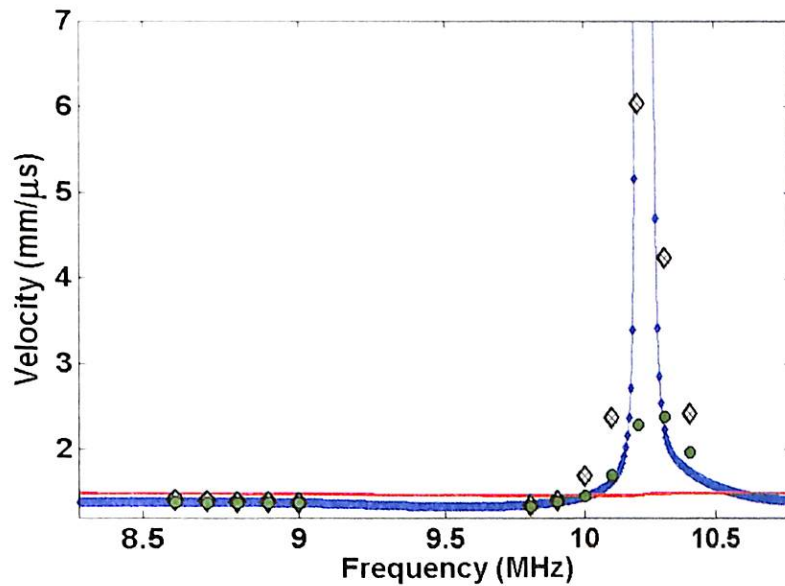


Figure 24: A comparison between the broadband and narrowband attenuation measurements for the Phase III data. The diamonds denote the center frequencies of the narrowband signals with a bandwidth of 0.10 MHz, and the dots denote the center frequencies of those signals with a bandwidth of 0.40 MHz. The 0.10 MHz bandwidth data reveal a greater increase in velocity as well as correspondence with the broadband values at frequencies between 10.0 and 10.4 MHz.

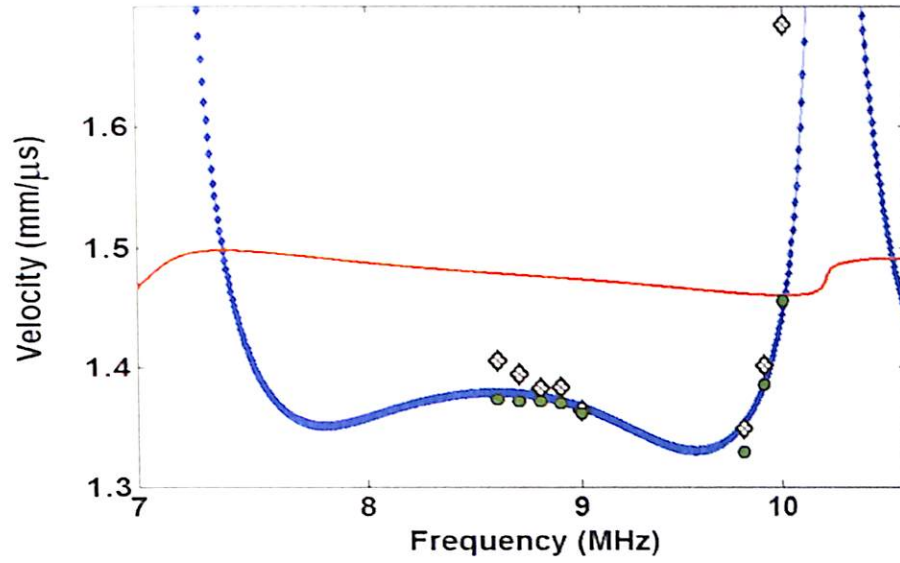


Figure 25: An expanded look at the group velocity data. The diamonds denote the center frequencies of the narrowband signals with a bandwidth of 0.10 MHz, and the dots denote the center frequencies of those signals with a bandwidth of 0.40 MHz. When the graph is zoomed in on the region between 7 and 11 MHz the deviation of the 0.10 MHz bandwidth data from the broadband data becomes apparent.

## DISCUSSION

The narrow size distribution of microspheres along with the resonances exhibited by the spheres across their scattering cross-sections account for the large dispersion observed in all of the measurements. From earlier work (Mobley, 2007a), calculations indicate a variation in the scattering-to-geometric cross section of the 160  $\mu\text{m}$  spheres from 0.1 at 2 MHz to 3.8 at 4.5 MHz. The region near 4.5 MHz shows a correspondence between the negative delay and a Q factor of 10. The first phase of the project verifies the prediction that negative group delays could exist in suspensions of similar volume fractions (Mobley, 2005). These measurements also verify that the suspension is significantly dispersive, even at a volume fraction of only 3%. The attenuation bands from this Phase I data are such that they can be easily identified experimentally while still varying by an order of magnitude across the region of interest. (Mobley, 2007a)

One issue that must be addressed is the fact that in Phase I of the project only broadband signals were used to make the measurements of attenuation and velocity. With broadband pulses there exists no directly observable feature in the time-domain that would point to the fact that the group delay became negative at any point. Directly observable time-domain features in narrowband pulses that indicate that the group delay is negative should exist, and investigating the directly observable time-domain features related to abnormal group velocities is the purpose for Phases II and III

One aspect of data analysis that has been incorporated into earlier work is the use of Kramers-Kronig relations which allow for the verification of consistency between the

dispersion and attenuation data extracted from the signals. Kramers-Kronig relations provide a means of calculating the group velocity directly from the attenuation coefficient, and have been shown to provide accurate predictions for microsphere data (Mobley 2005). Figure 26 shows the group delay of both the data and the predicted Kramers-Kronig spectrum. This spectrum shows the high level of agreement between the theoretical predictions and the actual measured spectrum verifying the Kramers-Kronig consistency of the experimental results of Phase I of the project.

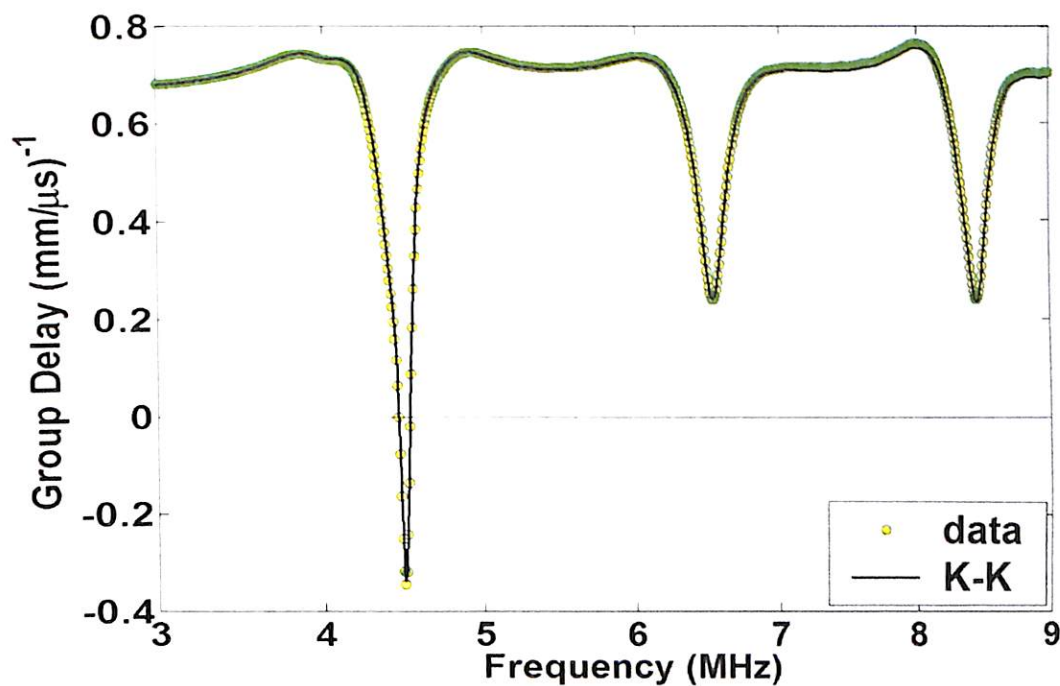


Figure 26: A comparison of the group delay spectrum of Phase I of the project with a Kramers-Kronig prediction using the attenuation coefficient for the input. The Kramers-Kronig prediction matches the data with a high level of agreement.



In Phase II a high level of consistency between the broadband data and the earlier Phase I result are observed. The same attenuation spectrum is observed with the most prominent peak occurring near 4.5 MHz. Additionally the phase delay time and the group delay time show agreement with earlier Phase I results. The narrowband results yield a trend that was anticipated, namely that the more narrowband the signal the closer the time-domain envelope amplitude and velocity will correspond to those measured by the broadband technique. In the case of the attenuation data, a high level of agreement is seen between the narrowband and broadband data across all the frequencies for the lower bandwidths. As bandwidth increases there is a greater deviation in attenuation values as the frequencies are changed. This trend is illustrated in Figure 27 which shows the agreement between the broadband and narrowband measurements. The higher the level of agreement, the closer the ratio falls to 1. For the bandwidth of 0.07 MHz nearly all of the frequency measurements have ratios that fall near 1 where as the higher bandwidths do not. The same idea can be seen in Figure 28 which compares the fractional differences between the narrowband and broadband results. The fractional difference is calculated using equation 8.

$$\frac{\alpha(f_c)_{\text{narrowband}} - \alpha(f_c)_{\text{broadband}}}{\alpha(f_c)_{\text{broadband}}} \quad (8)$$

The closer the data falls near the zero line indicates a higher level of agreement between the broadband and narrowband measurements. The fractional differences shown in Figure 28 illustrate the high level of agreement across all frequencies at lower bandwidths.

Figures 29 and 30 show the inconsistency of the group velocity of the broadband and narrowband signals. Across each bandwidth there is a varying level of agreement between the narrowband velocity and the accepted broadband velocity.

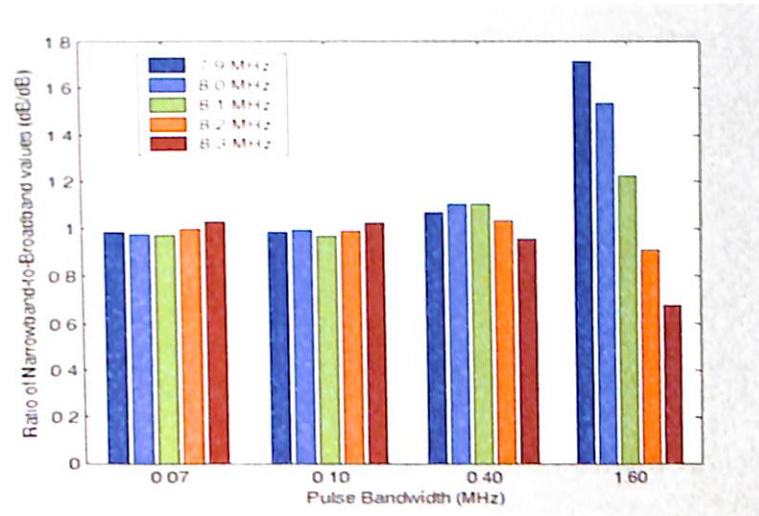


Figure 27: A ratio comparison of narrowband and broadband attenuation data of the 160 micron suspension for each frequency and bandwidth combination employed in Phase II of the project. The closer the ratio comes to 1 the higher the level of agreement between the broadband and narrowband values. A higher level of agreement across all the center frequencies is seen for lower bandwidths. This agreement decreases as bandwidth increases.

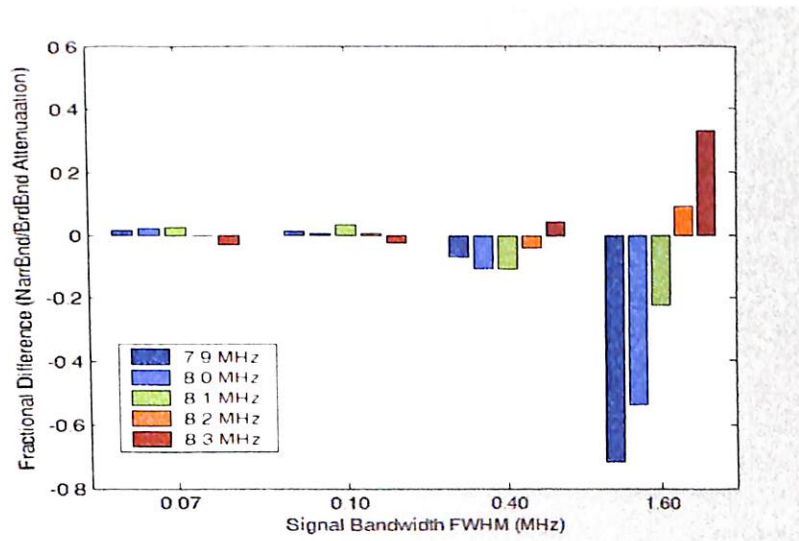


Figure 28: A fractional difference comparison of narrowband and broadband attenuation data of the 160 micron suspension for each frequency and bandwidth combination employed in Phase II of the project. The closer the values fall to zero the higher the level of agreement.

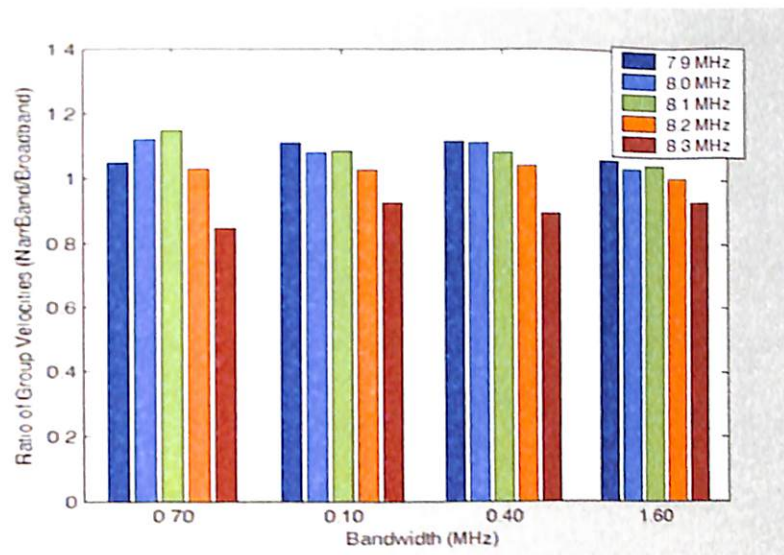


Figure 29: A ratio comparison of narrowband and broadband group velocity data of the 160 micron suspension for each frequency and bandwidth combination employed in Phase II of the project. A high level of agreement across all of the frequencies for the lower bandwidths is not seen as much as in the attenuation data.

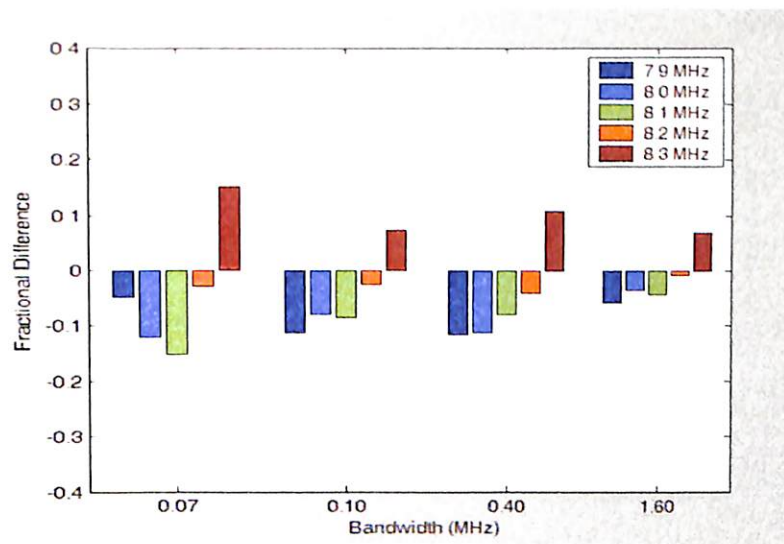


Figure 30: A fractional difference comparison of narrowband and broadband group velocity data of the 160 micron suspension for each frequency and bandwidth combination employed in Phase II of the project. The low level of broadband-narrowband agreement is depicted by the various differences displayed across the center frequencies of all of the bandwidths.

The broadband spectra are slightly different for Phase III due to the difference in diameter of the microspheres under study. Although the different sample displays different spectra, the general features of the data are the same. Notice that, as before, in regions of high attenuation the phase velocity decreases and then rapidly increases moving into regions of low attenuation. Additionally, the regions where the group delay becomes negative correspond to regions of high attenuation as was seen in the previous data. The details of the attenuation spectrum are different for this sample in that it shows several regions of higher attenuation than the lowest frequency band. Also the group delay curve becomes negative at a greater number of frequencies in this data than it does in the previous data.

The results of the group velocity measurements for both the broadband and narrowband data are summarized in Figures 31 and 32. Figure 31 depicts the data for the frequencies ranging from 8.6 to 9.0 MHz. The data show some agreement over that range of frequencies. Interestingly at the lower frequencies the 0.40 MHz bandwidth data shows a slightly higher level of agreement with the broadband data than does the 0.10 MHz bandwidth data. At 9.0 MHz the difference between the two bandwidths and the broadband values is small. Figure 32 shows a comparison of the narrowband and broadband data for the frequencies between 9.8 and 10.4 MHz. The data for the lower frequencies show a high level of agreement. At 10.2 MHz there is a drastic change in the agreement, and the lower bandwidth data (0.1 MHz) shows a higher level of agreement with the broadband data. This frequency falls in a region of high attenuation.

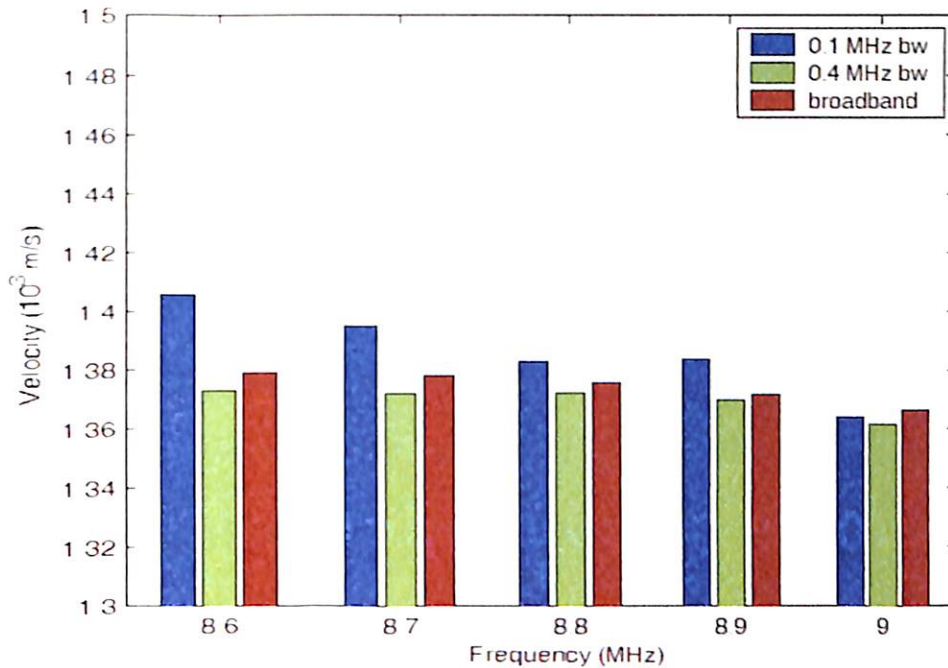


Figure 31: A comparison of the broadband and narrowband group velocity measurements of the 100 micron suspension of Phase III of the project. Frequency range: 8.6 to 9.0 MHz. The data show a higher level of agreement as frequency increases.

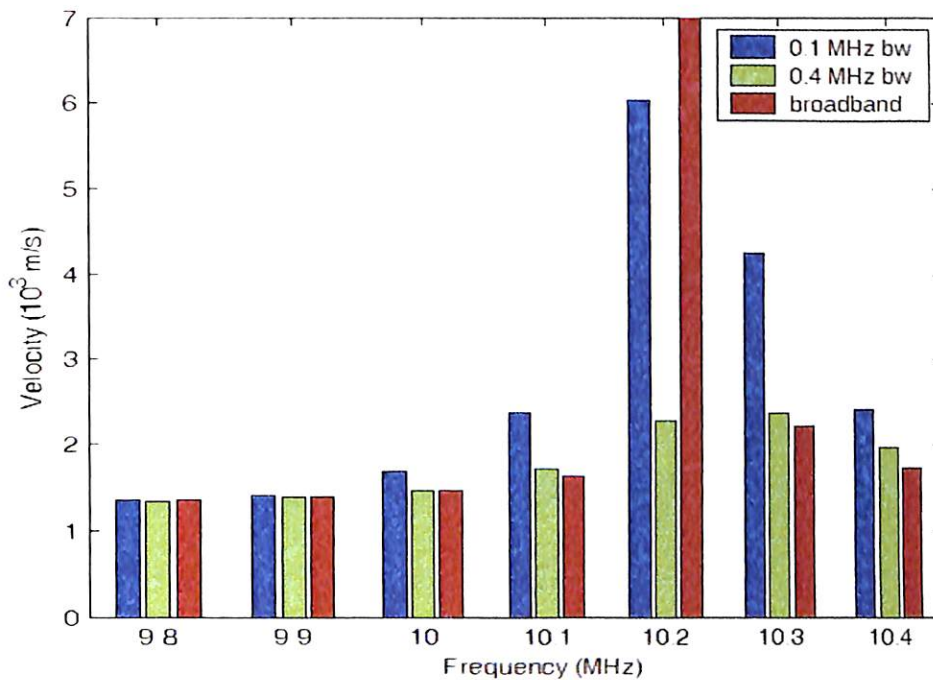


Figure 32: A comparison of the broadband and narrowband group velocity measurements of the 100 micron suspension of Phase III of the project. Frequency range: 9.8 to 10.4 MHz. The data display a high level of agreement at lower frequencies but begin to vary greatly around 10.2 MHz (a band of high attenuation).

## One Final Note

We know that even though our data show abnormal group velocities we are not in violation of Einstein's special theory of relativity that states no information can be transferred faster than the vacuum speed of light. The key to reconciling relativity and superluminal acoustic velocity lies in the understanding of the nature of the shaped acoustic pulses that we propagate. The signal can be thought of as a continuous sine wave of constant amplitude and is the substance of the wave (it physically exists). The envelope multiplies this and can be thought of as a shape that rides on top of the sine wave. The sine wave is cut off in time and travels at (or near to) the phase velocity. The envelope can travel at whatever speed it wants, but it can only exist when riding on top of the sine wave pulse because it has no physical existence of its own. So if it tries to outrun the sine waves it rides on, it ceases to exist.

Einstein's relativity states that information cannot travel faster than  $c$ , the speed of light in vacuum. We can think of the wave packet as a finite train of sine waves (the carrier) with some envelope (i.e., shape) imposed upon it. In the experiment our pulse can be thought of the signal that contains information encoded in the envelope, and the leading edge of the pulse determines the ultimate speed at which we can transfer this information. The pulse envelope (which effectively encodes some information onto its carrier) would have to somehow pass the leading edge in order for the information to be transmitted faster than our carrier wave. This, however, is not the case. When the wave propagates through the sample nothing can pass the leading edge of the wave packet that supports the envelope and travel faster than  $c$ , otherwise the principle of relativity will be violated. Although the envelope may be traveling at extreme speeds, it never actually

passes the leading edge of the wave. For the data that show the speed of the pulse envelope to be abnormally large and even greater than  $c$  no portion of the envelope actually ever passes the leading edge of the wave packet. When the envelope attempts to outrun the carrier, attenuation dampens it out effectively preserving the causal nature of the process. The envelope cannot travel beyond the carrier pulse that supports it, and therefore no information is actually transmitted faster than light. The edges of the pulse propagate at an ordinary acoustic velocity, and the laws of relativity are obeyed.

## CONCLUSION

In this project acoustic waves were used to measure dispersion properties of two suspensions that were shown to support superluminal group velocities. The suspension used in the first two phases of the project had a mean particle diameter of 160 microns, and the suspension used in the third phase had a mean particle diameter of 100 microns. In Phase I the suspensions were studied using broadband pulses with bandwidths from around 2 to 20 MHz. The group delay spectrum revealed that the suspensions do in fact support superluminal group velocities. These velocities occur near the negative delay region found near 4.5 MHz. The results of Phase I were also verified using Kramers-Kronig relations. During Phase II and III narrowband methods were used in order to obtain directly observable time domain measurements of abnormal velocities. The results of both phases showed a variation between the broadband and narrowband data. At certain frequencies and certain bandwidths the narrowband calculations have varying levels of agreement with the broadband results. None the less, the data do show abnormal group velocities.



## REFERENCES

J. Mobley and R. Heithaus, *Physical Review Letters* 90, 124301 (2007a).

Figures 9, 10, 11, 12, and 16 were derived from this work.

J. Mobley, K. R. Waters, and J. G. Miller, *Phys. Rev. E* **72**, 016604 (2005).

J. Mobley, *J. Acoust. Soc. Am.*, **121**, 1916 (2007b).

J. Mobley, "Ultrasonic Dispersion in Suspensions and Solids : A Study of  
Fundamental Dynamics and the Kramers-Kronig Relations." Washington Univ:  
1998.

J. Mobley, *J. Acoust. Soc. Am.* **118**, 1958 (2005); **122**, EL8 (2007c)

<http://www.acoustics.org/press/150th/Mobley.html>

R. Bracewell. *The Fourier Transform and its Applications*. 2<sup>nd</sup> edition. McGraw-Hill:  
New York 1986.

L. Brillouin, *Wave Propagation and Group Velocity* (Academic, New York, 1960).

## ADDITIONAL BIBLIOGRAPHY

- J. Mobley *et al.*, *J. Acoust. Soc. Am.* **106**, 652 (1999).
- S. Chu and S. Wong, *Phys. Rev. Lett.* **48**, 738 (1982).
- R. Y. Chiao and A. M. Steinberg, *Prog. Opt.* **37**, 347 (1997).
- L. Kinsler *et al.* Fundamentals of Acoustics, 4<sup>th</sup> edition. Wiley: New York 2000.
- D. Rachel. The Science and Applications of Acoustics. 2<sup>nd</sup> edition. Springer: New York 2007.
- G. M. Gehring *et al.* *Science* **312**, 895 (2006).
- A. Dogariu, A. Kuzmich, and L. J. Wang, *Phys. Rev. A* **63**, 053806 (2001).
- M. Mojahedi *et al.*, *IEEE J. Sel. Top. Quantum Electron.* **9**, 30 (2003).
- E. Recami, *et al.*, *IEEE J. Sel. Top. Quantum Electron.* **9**, 59 (2003).